*American Mineralogist, Volume 72, pages 337–344, 1987*

# Order-disorder in omphacitic pyroxenes: A model for coupled substitution in the point approximation

**Paula M. Davidson**
Ceramics Division, Institute for Materials Science and Engineering,
National Bureau of Standards, Gaithersburg, Maryland 20899, U.S.A.

**Benjamin P. Burton**
Metallurgy Division, Institute for Materials Science and Engineering,
National Bureau of Standards, Gaithersburg, Maryland 20899, U.S.A.

## Abstract

We develop a generalized point approximation for binary solutions that have coupled mixing on nonequivalent sites that may themselves be involved in coupled ordering transitions. For omphacite pyroxene solutions, ordering within the M1 sites is linked to ordering within M2 sites, so that disordering occurs at a single $T_c$ (critical temperature). In our model, coupled ordering in omphacites is achieved through both geometric and energetic parameters that account for the difference in cation-cation coordination number and the cross-site cation-pair-exchange energy $\Delta G^{\circ}_{ss}$. Although this model necessarily neglects short-range order, calculated phase-diagram topologies agree qualitatively with experiments and TEM observations. Differing degrees of long-range order are predicted at temperatures below $T_c$ for unequal intrasite ordering energies $W^{M1}$ and $W^{M2}$. Asymmetric or compositionally dependent functions for $\Delta G^{\circ}_{ss}$ complicate phase-diagram topologies and increase the possibility for stable coexistence of two ordered phases.

## Introduction

Since Clark and Papike (1968) showed that cation ordering in omphacites [with compositions near $(NaCa)(AlMg)Si_2O_6$] leads to a reduction in space-group symmetry from that of the disordered supergroup, $C2/c$, the order-disorder transition has become pivotal in the thermodynamic analysis of $NaAlSi_2O_6$-$CaMgSi_2O_6$ (jadeite-diopside; Jd-Di) pyroxene solutions. Thermodynamic models based on high-temperature phase equilibria (Ganguly, 1973; Gasparik, 1985) that treated $C2/c$ Jd-Di pyroxene as a binary one-site solution necessarily neglected the stability of ordered omphacites at temperatures below 700–850°C (estimated by Fleet et al., 1978). Transmission-electron microscopy (TEM) observations have helped to elucidate low-temperature phase relations involving natural ordered omphacites that are kinetically inaccessible to experiment. Phakey and Ghose's (1973) TEM observations of APBs (antiphase boundaries) in ordered omphacites are permissive evidence that the ordered phase inverted from a high-temperature disordered precursor. Subsequent observations by Carpenter (1978) of lamellar intergrowths of augite-omphacite, jadeite-omphacite, and two (ordered) omphacites led him to interpret phase relations (Carpenter, 1980) as shown in Figure 1.

Despite Carpenter's interpretations, there have been no attempts to model the phase relations with a generalized point (or Bragg-Williams) approximation (BW) that permits a higher-order transition from an ordered ($P$) to disordered ($C$) phase. Cohen (1986a) has applied a generalized pair approximation to the system but did not present a calculated phase diagram. The advantage of the pair approximation over the point approximation appears, however, to be chimeric: although it includes short-range order (SRO), it also predicts the stability of a $C2/c$ ground state with perfect SRO and *no* long-range order (LRO)![1] However, using the generalized point approximation and the energy parameters from Cohen and Burnham (1985), we calculate a symmetric model phase diagram that is similar to the one proposed by Carpenter (1980).

We have generalized the point approximation to treat coupled substitution in a double-site phase and have applied our model to omphacitic pyroxenes. This model produces allowable, alternative phase-diagram topologies and predicts solution enthalpies, cation distributions, and jadeite activities that are in qualitative agreement with experiment.

## Model development

### Symmetry considerations

The model we develop is general to binary solutions that have coupled mixing in nonequivalent sites, which

[1] This result violates the symmetry of omphacite by predicting an unfrustrated ground state in which all M1-M1 and M2-M2 nearest-neighbor pairs are in configurations Mg-Al and Ca-Na, respectively, but no M1-M2 pairs are in configurations Mg-Na or Al-Ca. This, of course, is geometrically impossible.

0003–004X/87/0304–0337$02.00

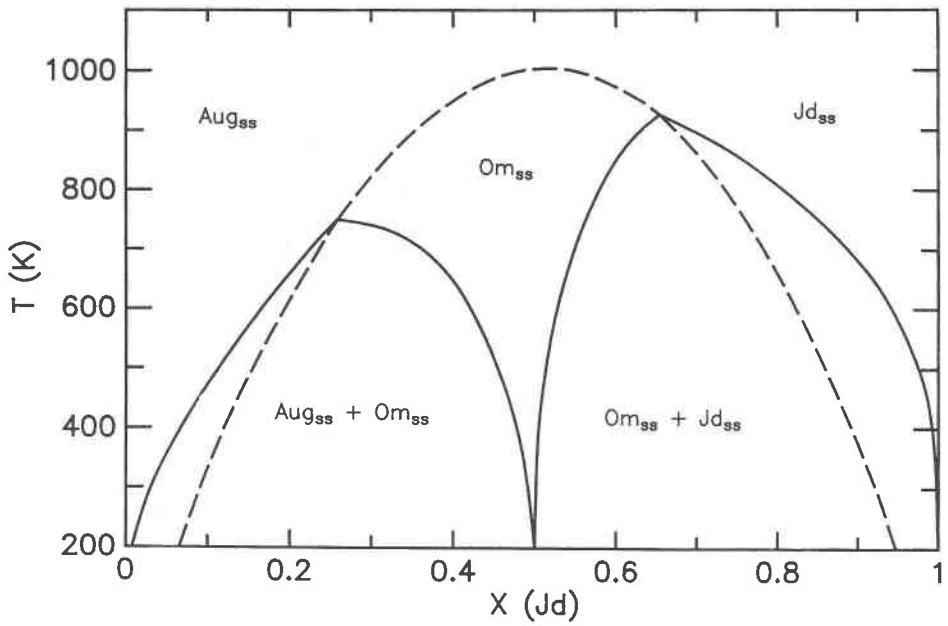


Fig. 1. *T-X* section for omphacite phase relations proposed by Carpenter (1978). The dashed line represents the order-disorder transition; solid curves indicate solvi between indicated phases. $Aug_{ss}$: augite solid solution (Di-rich, disordered *C2/c* pyroxene); $Om_{ss}$: omphacite solid solution (ordered *P2/n* pyroxene); $Jd_{ss}$: jadeite solid solution (Jd-rich, disordered *C2/c* pyroxene).

may themselves be involved in coupled ordering transitions. Such solutions are common among important mineral groups including feldspars and spinels. Application of our model to these systems should be straightforward; the zeroth-level approximation yields tractable expressions for quantitative fitting to experimental data and produces phase-diagram topologies in which higher-order phase transitions intersect miscibility gaps. These intersections may produce tricritical points or critical end points depending on relative strengths of pair energies (Meiering, 1963; Allen and Cahn, 1972; Inden, 1974).

We have imposed two restrictions on our model that

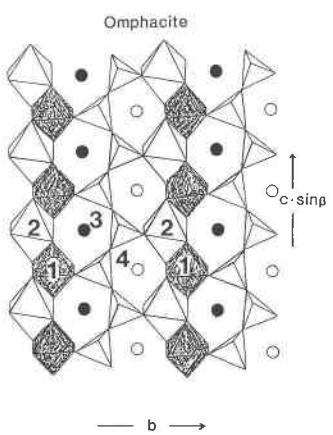


Fig. 2. Omphacite polyhedral layer projected down [100]. M1 sites are octahedra labeled 1 and 2; M2 sites are circles labeled 3 and 4. Darkened locations are occupied preferentially by Al [M1(1)] and Na [M2(3)]. After Clark and Papike (1968).

are specific to the structural details of omphacites, shown in Figure 2: (1) Pairwise M1(1)–M2(3) and M1(1)–M2(4) interaction energies are the same for identical species. Although M1(1)–M2(3) and M1(1)–M2(4) bond lengths differ slightly, the corresponding energy parameters calculated by Cohen and Burnham (1985) are not significantly different. (2) Cation distributions within M sites are linked both geometrically and energetically. Clark and Papike (1968) demonstrated that the ordering of Mg and Al into distinct M1 sites at low temperatures is accompanied by weaker ordering of Na and Ca within the M2 site, probably as a means of preserving local charge balance. When the symmetry of M1 sites is destroyed (by differing site occupancies), the M2 sites must also split into two crystallographically distinct sites: half the M2 sites are surrounded by two Al-rich sites plus one Mg-rich site, and half are surrounded by two Mg-rich sites plus one Al-rich site. Observations that the Na-Ca distributions are more disordered than Mg-Al distributions can be corroborated in our model by different ordering energies. However, the change of symmetry requires that (LRO) in both M1 and M2 sites disappears at the parameter of the *P–C* transition. Our model incorporates this restriction for structures that have differing coordination numbers among sites in the ordered phase or nonzero net cross-site pair interaction energy, $\Delta G^{\circ}_{2}$ (defined below).

### Enthalpy of mixing

The idealized projection down [100] of the omphacite polyhedral layer (Fig. 2) shows all nearest-neighbor M-site locations. Coordination numbers $Z_{ij}$, where $i$ and $j$ are the site indices as labeled in Figure 2, are given in Table

1. Cation-cation interactions within each M site contribute to enthalpy according to the familiar BW expression

$$H(\mathrm{M1,M1}) = (1/Z_{12})(n_{\mathrm{AlAl}}\omega_{\mathrm{AlAl}} + n_{\mathrm{AlMg}}\omega_{\mathrm{AlMg}} + n_{\mathrm{MgMg}}\omega_{\mathrm{MgMg}}) \quad (1a)$$

$$H(\mathrm{M2,M2}) = (1/Z_{34})(n_{\mathrm{NaNa}}\omega_{\mathrm{NaNa}} + n_{\mathrm{NaCa}}\omega_{\mathrm{NaCa}} + n_{\mathrm{CaCa}}\omega_{\mathrm{CaCa}}), \quad (1b)$$

where $n_{\mathrm{AlAl}}$ is the number of Al-Al pairs per 2 mol of M1 sites, and $\omega_{\mathrm{AlAl}}$ is their pairwise interaction enthalpy, and similarly for the other cation pairs. All thermodynamic quantities are expressed per mole $M1_2M2_2Si_4O_{12}$. Interactions between M1-site cations and M2-site cations, allowing for the differences in coordination numbers, contribute the following enthalpy:

$$\begin{aligned} H(\mathrm{M1,M2}) = {} & (1/Z_{13})(n_{\mathrm{AlNa}}\omega_{\mathrm{AlNa}} + n_{\mathrm{AlCa}}\omega_{\mathrm{AlCa}} + n_{\mathrm{MgNa}}\omega_{\mathrm{MgNa}} + n_{\mathrm{MgCa}}\omega_{\mathrm{MgCa}}) \\ & + (1/Z_{14})(n_{\mathrm{AlNa}}\omega_{\mathrm{AlNa}} + n_{\mathrm{AlCa}}\omega_{\mathrm{AlCa}} + n_{\mathrm{MgNa}}\omega_{\mathrm{MgNa}} + n_{\mathrm{MgCa}}\omega_{\mathrm{MgCa}}) \\ & + (1/Z_{23})(n_{\mathrm{AlNa}}\omega_{\mathrm{AlNa}} + n_{\mathrm{AlCa}}\omega_{\mathrm{AlCa}} + n_{\mathrm{MgNa}}\omega_{\mathrm{MgNa}} + n_{\mathrm{MgCa}}\omega_{\mathrm{MgCa}}) \\ & + (1/Z_{24})(n_{\mathrm{AlNa}}\omega_{\mathrm{AlNa}} + n_{\mathrm{AlCa}}\omega_{\mathrm{AlCa}} + n_{\mathrm{MgNa}}\omega_{\mathrm{MgNa}} + n_{\mathrm{MgCa}}\omega_{\mathrm{MgCa}}), \quad (1c) \end{aligned}$$

where, for example, $n$AlNa is the fraction of Al[M1$_i$]-Na[M2$_j$] pairs and sites $i$ and $j$ are given in the coefficients $1/Z_{ij}$. We may define $s_1$ as the LRO parameter for the M1 site, such that $X + Xs_1$ is the fraction of the M1$\alpha$ site occupied by Al and $X$ is the mole fraction of jadeite. Then $s_1 = 0$ gives the completely disordered M1-site cation distribution, and for $X$ not greater than ½, $s_1 = 1$ gives the maximally ordered M1-site cation distribution; $s_2$ is the corresponding M2-site LRO parameter. Substituting the appropriate products of cation-site occupancies listed in Table 2 for the numbers of pairs in (1) yields the following enthalpy for omphacite solutions:

$$\begin{aligned} H^{\mathrm{sol}} = {} & X\mu^0_{\mathrm{Jd}} + (1 - X)\mu^0_{\mathrm{Di}} \\ & + W^{\mathrm{M1}}[(Xs_1)^2 + X(1 - X)] \\ & + W^{\mathrm{M2}}[(Xs_2)^2 + X(1 - X)] \\ & + \Delta G^0_{\mathrm{ex}}[2X(1 - X) - \Delta Z(X(1 - X) + X^2 s_1 s_2))] \end{aligned}$$

where $\Delta Z = (Z_{13} - Z_{14})/Z_{13}$ (= ½), $W^{\mathrm{M1}} = (1/Z_{12})[2\omega_{\mathrm{AlMg}} - \omega_{\mathrm{AlAl}} - \omega_{\mathrm{MgMg}}]$; $W^{\mathrm{M2}} = (1/Z_{34})[2\omega_{\mathrm{NaCa}} - \omega_{\mathrm{NaNa}} - \omega_{\mathrm{CaCa}}]$; $\Delta G^0_{\mathrm{ex}} = (1/Z_{14})[\omega_{\mathrm{AlCa}} + \omega_{\mathrm{MgNa}} - \omega_{\mathrm{AlNa}} - \omega_{\mathrm{MgCa}}]$. The coefficients of $X$ and $1 - X$ are standard-state energies, so that the last three lines of the above expression constitute the mixing enthalpy. Note that for ordered omphacites, the M1–M2 interaction energy $\Delta G^0_{\mathrm{ex}}$ contributes cooperatively to enthalpy only because the coordination number difference $\Delta Z$ is nonzero. The signs of $W^{\mathrm{M1}}$ and $W^{\mathrm{M2}}$ are negative, to promote ordering within M sites, and the sign of $\Delta G^0_{\mathrm{ex}}$ is positive to favor phase separation into Di-rich and Jd-rich solutions.

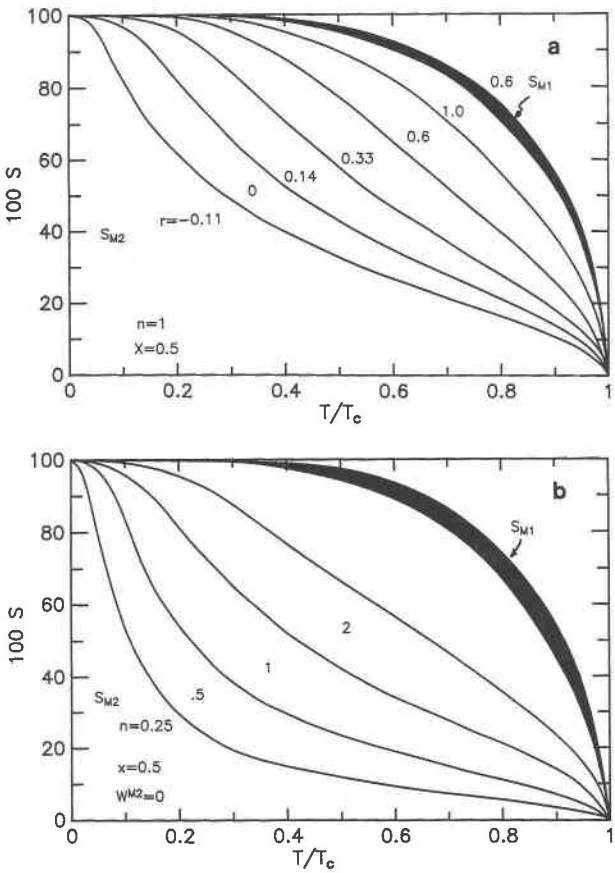


Fig. 3. $s$ vs. $T/T_c$. (a) $n = 1$; $r$ values are indicated next to curves, which are all for $s_2$ except the one labeled $S_{M1}$. $s_1$ values for $r < 0.6$ are located in the shaded envelope. (b) $r = 0$; $n$ values are indicated next to curves which are all for $s_2$ except that labeled s(M1). $s_1$ values for $0 < n < 2$ are located in the shaded envelope.

## Configurational entropy

Configurational entropy in the BW approximation is simply expressed by $S^{\mathrm{mix}} = -R[\Sigma\, X^{ij} \ln X^{ij}]$ where the site occupancies $X^{ij}$ are given as functions of $X$, $s_1$, and $s_2$ in Table 2.

TABLE 1. Coordination numbers

| | M1$\alpha$ | M1$\beta$ | M2$\alpha$ | M2$\beta$ |
|---|---|---|---|---|
| M1$\alpha$ | — | $Z_{12} = 2$ | $Z_{13} = 2$ | $Z_{14} = 1$ |
| M1$\beta$ | | — | $Z_{23} = 1$ | $Z_{24} = 2$ |
| M2$\alpha$ | | | — | $Z_{34} = 2$ |
| M2$\beta$ | | | | — |

TABLE 2. Site occupancies

| | M1$\alpha$ | M1$\beta$ | M2$\alpha$ | M2$\beta$ |
|---|---|---|---|---|
| Al | $X + Xs_1$ | $X - Xs_1$ | | |
| Mg | $1 - X - Xs_1$ | $1 - X + Xs_1$ | | |
| Na | | | $X + Xs_2$ | $X - Xs_2$ |
| Ca | | | $1 - X - Xs_2$ | $1 - X + Xs_2$ |

### Order-disorder

Equilibrium values for the LRO parameters, $s_{1eq}$ and $s_{2eq}$, are found by minimizing the free energy $G$ with respect to $s_1$ and $s_2$:

$$\partial G/\partial s_1 = 0$$
$$= 2X^2 s_1 W^{M1} - \Delta Z X^2 s_2 \Delta G^0_{ss} + XRT \cdot \ln\{[(1 - X + Xs_1)(X + Xs_1)]/[(1 - X - Xs_1)(X - Xs_1)]\} \quad (2a)$$

$$\partial G/\partial s_2 = 0$$
$$= 2X^2 s_2 W^{M2} - \Delta Z X^2 s_1 \Delta G^0_{ss} + XRT \cdot \ln\{[(1 - X + Xs_2)(X + Xs_2)]/[(1 - X - Xs_2)(X - Xs_2)]\} \quad (2b)$$

In the real systems, $S_{1eq} \neq S_{2eq}$ (in general) for $0 < T < T_c$, and it can be seen from Equations 2a and 2b that we predict $S_{1eq} = S_{2eq}$ if and only if $W^{M1} = W^{M2}$. Space-group symmetry requires, however, that the ordering on M1 and M2 sites be coupled in such a way that $s_1 \to 0$ implies $s_2 \to 0$, and vice versa, which means that there is only one $T_c$. This constraint is related to the second terms in Equations 2a and 2b, which imply that $s_1 = f(s_2)$ and $s_2 = f(s_1)$. If either $\Delta Z$ or $\Delta G^0_{ss}$ were equal to zero, then $s_1$ and $s_2$ would be independent and two $T_c$ values would be possible. Note that if we solve Equation 2b for $s_1$, when $s_2 \to 0$, $s_1$ must also vanish. Similarly, solving Equation 2a for $s_2$ shows that $s_1 = 0$ implies $s_2 = 0$.

Differences in $s_{1eq}$ and $s_{2eq}$ increase with decreasing values of the ratios $W^{M2}/W^{M1}$ ($\equiv r$) and $\Delta G^0_{ss}/(W^{M1} + W^{M2})$ ($\equiv -n$), as shown in Figures 3a and 3b. The latter variation is readily explained as a consequence of decreasing the coupling energy between M1 and M2 sites, by decreasing the energetic penalty for producing Al-Ca and Mg-Na pairs.

This model—like other double-sublattice, but noncoupled ordering, models—has two solutions for $(s_1,s_2)$ below $T_c$: $s_1,s_2 = (0,0)$ and $s_1,s_2 = (s_{1eq},s_{2eq})$ but only one solution at $T > T_c$: $s_1,s_2 = (0,0)$. For $T < T_c$, the solution that minimizes $G$ is of course that providing nonzero (ordered) values of $s_1$ and $s_2$ because the stability function $(\partial^2 G/\partial s_1^2)(\partial^2 G/\partial s_2^2) - (\partial^2 G/\partial s_1 \partial s_2)^2$ is positive. For $s_1 = s_2 \to 0$, setting the stability function equal to zero defines the ordering temperature $T_c$ as a function of $X$:

$$T_c = \frac{X(1 - X)}{2R}\{-[W^{M1} + W^{M2}] \pm [(W^{M1} - W^{M2})^2 + (\Delta Z \Delta G^0_{ss})^2]^{1/2}\}. \quad (3)$$

Notice that for $\Delta Z$ and/or $\Delta G^0_{ss} = 0$, there are two transition temperatures: $T_{c_1} = -X(1 - X)W^{M1}/R$ and $T_{c_2} = -X(1 - X)W^{M2}/R$ corresponding to independent disordering within each site. For omphacites, the lower value for $T_c$ obtainable from Equation 3 is not physically meaningful because it defines a sign change in the stability function for nonequilibrium values of $(s_1,s_2)$.

### Phase-diagram topology

For $T < T_c$, the ordered phase is stable relative to the disordered phase, but may not be stable relative to a two-phase assemblage including an ordered phase with $X \approx 0.5$ plus either an ordered phase or a disordered phase of more extreme composition. Allen and Cahn (1982) have shown that when the spinodal $T_c(X)$ associated with ordering intersects the conditional spinodal $T_{so}(X)$ associated with phase separation of the *ordered* phase, a tricritical point occurs if the signs of $dT/dX$ for the spinodals are opposite. When the spinodals have the same sign for $dT/dX$, a critical end point occurs where the ordering spinodal intersects a miscibility gap between two ordered phases. The tricritical-point topology is replaced by critical-end-point topology when $(dT_{so}/dX)/(dT_c/dX) \to 0$. In our model, this "critical ratio" has a complicated dependence on energy parameters. However, we have empirically found that for $n = -\Delta G^0_{ss}/(W^{M1} + W^{M2}) < \sim 0.45$ and $\Delta G^0_{ss} \neq f(X)$, critical end points, rather than tricritical points, result.

At 0 K, omphacite is stable relative to an assemblage of Di + Jd for values of $n \leqq 2$. For $n > 2$, coexisting disordered Di-rich and Jd-rich solutions are more stable than ordered omphacite. The temperature $T_s$ of the spinodal associated with phase separation of two disordered phases is given by $\partial^2 G/\partial X^2 = 0$ for $s_1$ and $s_2 \to 0$, or

$$2RT_s = X(1 - X)[W^{M1} + W^{M2} + \Delta G^0_{ss}(2 - \Delta Z)]. \quad (s_1 = s_2 = 0)$$

For $\Delta Z = \frac{1}{2}$, $T_c \geqq T_s$ over all $X$ for $n = 2$. Thus, this model in its compositionally symmetric limit cannot produce a phase-diagram topology in which an ordered-phase stability field pinches out to a stability field for two disordered phases with increasing temperature. These results are summarized in Figure 4, which shows systematic variations of phase-diagram topologies with $n$ and $r$.

Phase-diagram topologies are affected by variations in $r$, reflecting differences in strength of intrasite ordering. In Figure 4 we show that as $r$ approaches zero, the stability fields for all topologies are shifted to higher values of $n$.

### Asymmetric extension

In order to account for the marked compositional asymmetry in many binary systems, we could include asymmetry (compositional dependence) in any or all three interaction energies. We have substituted the compositionally dependent function $\Delta G^0_1 + X\Delta G^0_2$ for $\Delta G^0_{ss}$, in order to explore the effects of asymmetry, because in the disordered phase, the M1–M2 interaction mimics deviations from ideality in a regular solution. Including asymmetry as $\Delta G^0_1 + X\Delta G^0_2$ is similar to applying an asymmetric Margules model where $G^{ex} = W_{G1}X(1 - X)^2 + W_{G2}X^2(1 - X) = X(1 - X)[W_{G1} + X(W_{G2} - W_{G1})]$. For

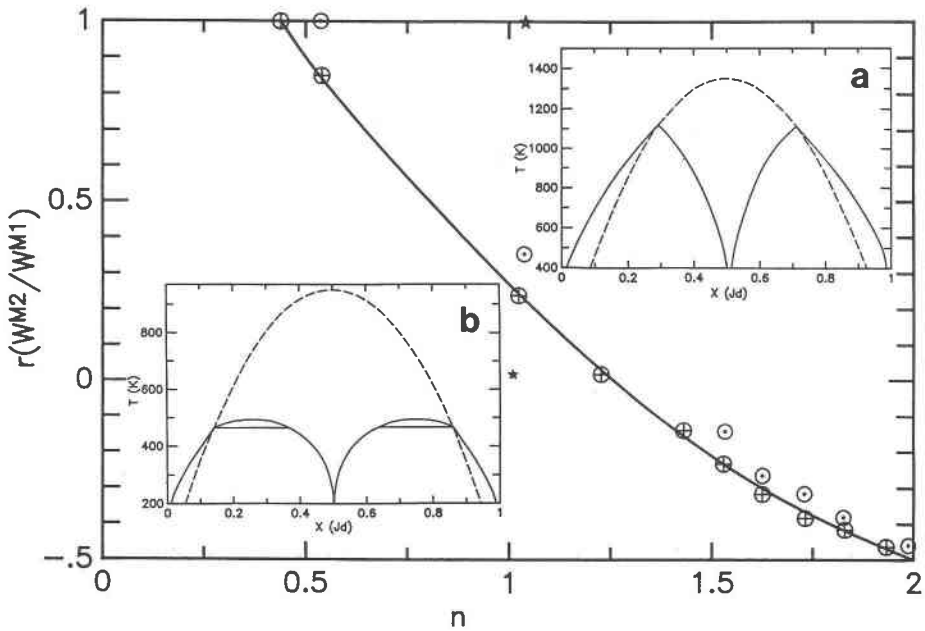


Fig. 4. Phase-diagram topologies: $\Delta G_2^0 = 0$. ⊕ indicates the topology shown in the inset $T$-$X$ section (a). ⊙ indicates the topology shown in the inset $T$-$X$ section (b). The dashed line is an estimate of the boundary between the two topology fields. For $n \geqq 2$, the ordered phase is metastable with respect to an assemblage of two disordered phases.

$T > T_c$, this model has the same functional form as the two-site models previously employed by Wood et al. (1980), Holland (1983), Gasparik (1985), and Cohen (with modifications, 1986b).

Additional phase-diagram topologies become possible with increasing asymmetry, as illustrated in Figures 5 ($r$ = 1) and 6 ($r$ = 0). Because the spinodals associated with ordering and with phase separation in the disordered phase adopt different compositional maxima in asymmetric models, a stability field for two disordered phases is created at sufficiently large $n$ and $\Delta G_2^0/\Delta G_1^0 \equiv q$. With increasing asymmetry and $n > \sim 1.35$, the sequence of phase-diagram topologies is topologically equivalent to the sequence of Figures 5a, 5c, 5d, and 5e. Depending on the ratio of intrasite-interaction energies, a field for coexisting ordered phases develops at lesser asymmetry ($r$ = 0) or greater asymmetry ($r$ = 1) than that for two disordered phases.

## Discussion

### Comparison with theoretical phase-diagram topologies

Our model is generalized from the point approximation and, for limiting values of $\Delta Z$ and $r$, may be compared to BW models for ordering in the CsCl structure (Allen and Cahn, 1972; Inden, 1974) and for magnetic transitions in immiscible binary alloys (Meiering, 1963). Allen and Cahn's generalized point approximation includes first and second nearest-neighbor interactions. In the CsCl structure, pair-formation energies within each sublattice are equal, but positive; the cross-site interaction is negative. The limiting ratio for stability of an ordered phase ($n \leqq 2$) corresponds to Allen and Cahn's (1982) ratio of second nearest-neighbor to first nearest-neighbor energies $V_2/V_1 < (-4/9)$.

Meiering (1963) predicted phase-diagram topologies for binary alloys of a magnetic plus a nonmagnetic component. Using a BW approximation for the magnetic-ordering transition and a regular solution model for immiscibility in the nonmagnetic phase, he found that for increasing ratios of ordering energy to unmixing energy, consolute points for coexisting disordered phases are joined and then replaced by tricritical points. Meiering was concerned with the analogue of only half of the system Di-Jd ($X_{Jd}$ = 0.5–1); decreasing the magnitude of ordering energy relative to unmixing energy is analogous in our model to increasing the asymmetry ratio $q$ relative to ordering energy. This sequence of topologies is illustrated in Figure 5. At very large values of $q$, the composition of the ordered phase in equilibrium with two disordered phases moves to values of $X_{Jd}$ that are less than 0.5. It then intersects and becomes metastable with respect to the assemblage of ordered + disordered phases ($X < 0.5$ for both phases).

### Comparison with observations

TEM. As illustrated in Figures 4–6, for the majority of energy-parameter choices, the resulting phase-diagram topology includes two coexisting ordered phases for $X < 0.5$ (where $\Delta G_2^0$ is smaller and critical points are at lower $T$ than their counterparts for $X > 0.5$). The likelihood for such topologies is greater for larger differences in intrasite-ordering energy and for larger asymmetry. Car-

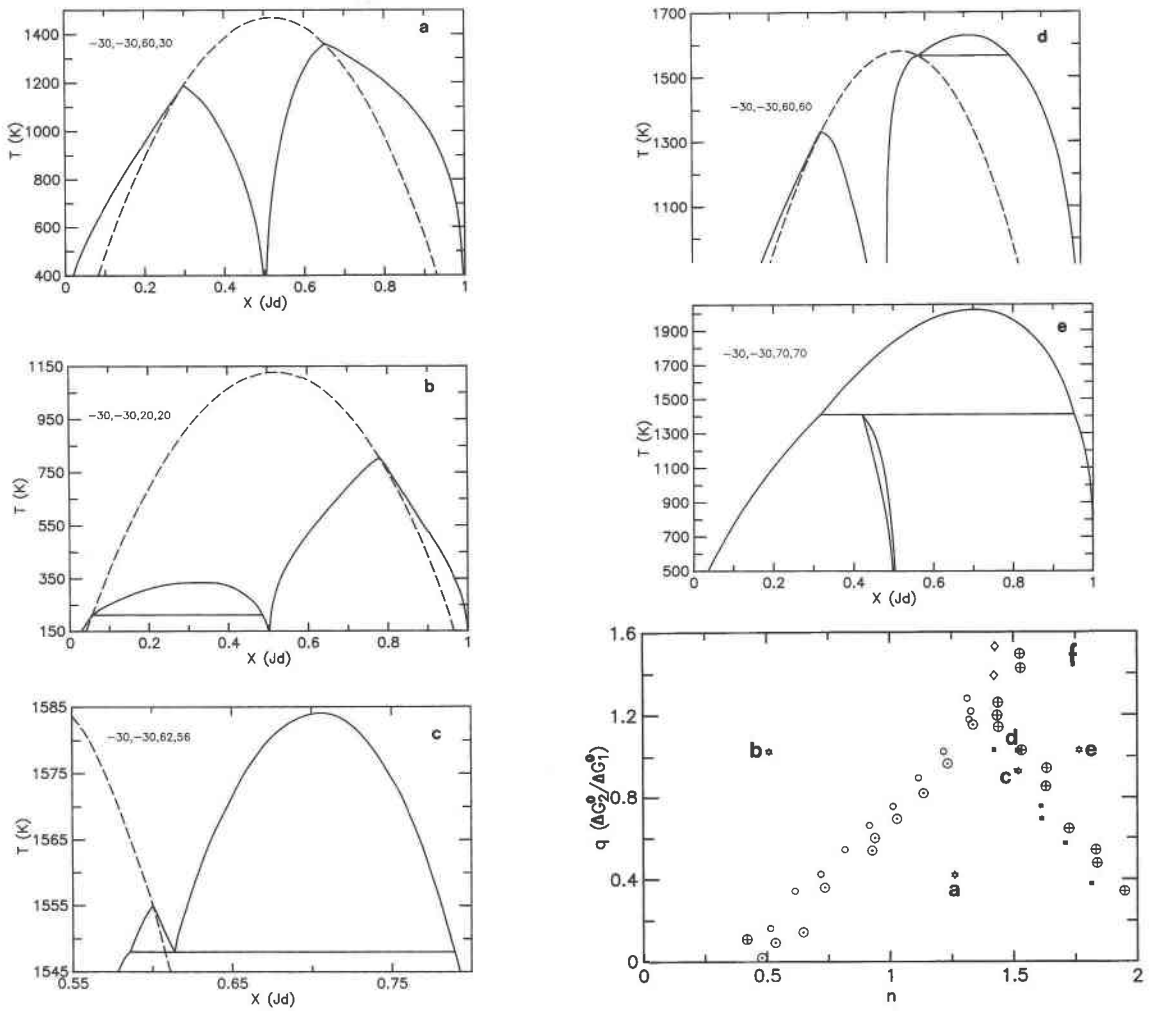


Fig. 5. Phase-diagram topologies: $r = 1$. (a)–(e) Representative phase diagrams calculated for energy parameters [$W^{M1}$, $W^{M2}$, $\Delta G^{\circ}_1$, $\Delta G^{\circ}_2$] (kJ/mol) as labeled. (f) Topologies vs. $q$ and $n$; ratios for (a)–(e) are plotted as stars. Topology (a) shown by ⊙; topology (b), ○; topology (c), ■; topology (d), ⊕.

penter's (1978) TEM observations of intergrown ordered omphacites for *diopside*-rich bulk compositions in addition to lamellar intergrowths of ordered plus disordered phases are consistent with the sense of asymmetry in mixing properties, apparent in calorimetric and phase-equilibrium experiments discussed below. Carpenter's interpretation, that the intergrown, ordered omphacites represent a quenched, metastable assemblage, may be broadened to include the possibility of a quenched, stable assemblage of two ordered phases.

**Calorimetric measurements.** Wood et al. (1980) measured solution enthalpies of disordered Di-Jd pyroxenes synthesized at 1350°C and 30 kbar. Our model for mixing enthalpy of the disordered phase can be compared to theirs, yielding $[W^{M1} + W^{M2} + (\frac{1}{2})\Delta G^{\circ}] = 61$ kJ/mol ($M1_2M2_2Si_4O_{12}$) or $38 + 20X_{Jd}$ (Holland, 1983) or $42 + 27X_{Jd} - 66X^2_{Jd}$ (Cohen, 1986b, after reinterpreting the mechanical mixing contribution to Wood et al.'s results). Furthermore, the enthalpy of disordering a natural specimen, ~16 kJ/mol (Wood et al.), constrains the energy parameters as follows: $\Delta H_{S=0} - \Delta H_{S=1} = [\Delta G^{\circ}/2 - W^{M1} - W^{M2}]/4 = (1 + n/2)[W^{M1} + W^{M2}]/4 > 16$ kJ/mol. Therefore, $\sim -64 < W^{M1} + W^{M2} \leqq -32$ (kJ).

**Jd + Q = Ab equilibria.** Experimental determinations of the reaction Jd + Q = Ab (e.g., Holland, 1983; Gasparik, 1985) constrain activities of Jd in the pyroxene solution through the isothermal displacement of the pressure $P^0$ for the endmember reaction $P^0 - P = [RT \ln(a_{Jd})]/\Delta V^0_{P,T}$ where $\Delta V^0_{P,T}$ is the endmember volume change for the reaction at $P$ and $T$; here assumed to be unchanged from that at 1 bar, 298 K. Holland noted that his 600°C experiments on the displacement suggest substantial ordering for $X_{Jd}$ near 0.5, owing to enhanced stability of pyroxenes relative to Jd-rich or Di-rich compositions. Since no LRO was observed, the stabilization was attributed to SRO. Gasparik's (1985) 1200–1350°C experiments on this reaction do not show any ordering stabilization. He argued, however, for the persistence of

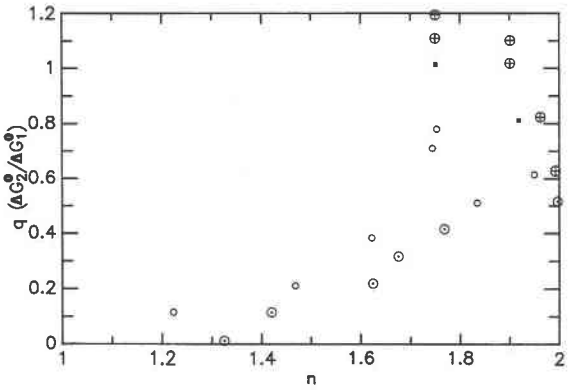


Fig. 6. Phase-diagram topologies: $r = 0$. Symbols as in 5.

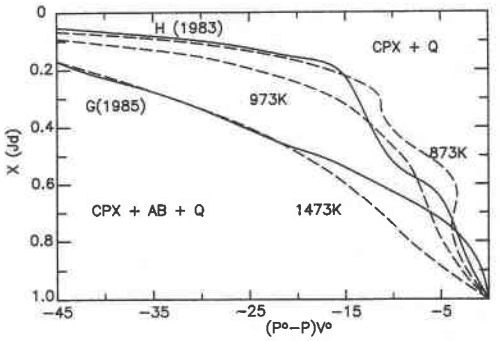


Fig. 7. $(P^0 - P)\Delta V^0$ vs. $X_{Jd}$ for the reaction Ab ⇌ Jd + Q. $P^0$ and $\Delta V^0$ represent the pressure and volume change of the reaction for the Jd endmember. Solid curves are smoothed from experiments at 873 K (Holland, 1983) and 1473–1623 K (Gasparik, 1985). Dashed curves are model calculations for the energy parameters [−29, −8,50, 13.5] (kJ/mol) and indicated temperatures.

nonnegligible SRO at these temperatures on the basis of model entropies that are lower than predicted by a random, two-site model. Figure 7 shows the experiments of Holland (1983) and Gasparik (1985) plotted as $(P^0 - P)\Delta V^0$ vs. $X_{Jd}$. The high-temperature experiments show little temperature-dependence, suggesting that cooperative ordering is not contributing substantially to activity at these temperatures. Also, there is no observable stabilization of intermediate compositions. Alternatively, the temperature range of the experiments may be too limited for an observable temperature-dependence in the isothermal $P$ displacements.

Also shown in Figure 7 are calculated values for $RT \cdot \ln(a_{Jd})$ vs. $X$ for the parameter set $\{W^{M1}, W^{M2}, \Delta G_1^0, \Delta G_2^0\} = \{-29, -8, 50, 13.5\}$ (units: kJ/mol). This set was optimized to fit solution enthalpies, phase equilibria, and $T_c \sim 850$°C (Carpenter, 1981) by using starting values based on the above constraints for the disordered-solution enthalpies and Cohen and Burnham's (1985) SRO energies. It is apparent from Figure 7 that the overestimate of entropy in our generalized point approximation can be compensated by solution enthalpies (that agree with measurements) to achieve a good fit to phase equilibria at $X < \sim 0.6$.

### Higher-order approximations

The neglect of SRO is an inherent shortcoming of this model that prevents us from quantitatively fitting Holland's (1983) 600°C experiments involving equilibrium between metastably short-range-ordered omphacites, plagioclase, and quartz. By including SRO, we can expect to improve (reduce) the estimate of configurational entropy in the disordered phase and corresponding enthalpy. Provided appropriate symmetry constraints can be applied, SRO will not affect ground-state assemblages at 0 K (where SRO is perfect).

## Conclusions

Omphacite solution models based on coupled substitutions in two nonequivalent sites yield, in the zeroth-level approximation, phase-diagram topologies that agree qualitatively with observation. Ordering within the M1 and M2 sites is *coupled* by the difference in coordination number $Z$, and this leads to simultaneous loss of LRO at a single $T_c$. Differing degrees of LRO within each site are predicted for $0 < T \leqq T_c$ when the intrasite-ordering energies are unequal ($W^{M1} \neq W^{M2}$). Asymmetric or compositionally dependent functions for $\Delta G_2^0$ complicate phase-diagram topologies and increase the possibility for coexisting ordered phases.

## Acknowledgments

We thank M. A. Carpenter, R. E. Cohen, and Tibor Gasparik for valuable discussion and reviews of this paper. This work was supported in part by the National Research Council program for postdoctoral associateships.

## References

Allen, S.M., and Cahn, J.W. (1972) Ground state structures in ordered binary alloys with second neighbor interactions. Acta Metallurgica, 20, 423–433.

Allen, S.M., and Cahn, J.W. (1982) Phase diagram features associated with multicritical points in alloy systems. Bulletin of Alloy Phase Diagrams, 3, 287–295.

Carpenter, M.A. (1978) Kinetic control of ordering and exsolution in omphacites. Contributions to Mineralogy and Petrology, 67, 17–24.

——— (1980) Mechanisms of exsolution in sodic pyroxenes. Contributions to Mineralogy and Petrology, 71, 289–300.

——— (1981) Time-temperature-transformation (TTT) analysis of cation disordering in omphacite. Contributions to Mineralogy and Petrology, 78, 433–440.

Clark, J.R., and Papike, J.P. (1968) Crystal-chemical characterization of omphacites. American Mineralogist, 53, 840–868.

Cohen, R.E. (1986a) Configurational thermodynamics of aluminous pyroxenes: A generalized pair approximation. Physics and Chemistry of Minerals, 13, 183–197.

——— (1986b) Thermodynamic solution properties of aluminous clinopyroxenes: Nonlinear least-squares refinements. Geochimica et Cosmochimica Acta, 50, 563–575.

Cohen, R.E., and Burnham, C.W. (1985) Energetics of ordering in aluminous pyroxenes. American Mineralogist, 70, 559–567.

Fleet, M.E., Herzberg, C.T., Bancroft, G.M., and Aldridge, L.P. (1978) Omphacite structural studies: I. The $P2/n \rightarrow C2/c$ transition. American Mineralogist, 63, 1100–1106.

Ganguly, J. (1973) Activity-composition relation of jadeite in omphacite

pyroxene: Theoretical deductions. Earth and Planetary Sciences Letters, 19, 145–153.

Gasparik, T. (1985) Experimentally determined compositions of diopside-jadeite pyroxene in equilibrium with albite and quartz at 1200–1350°C and 15–34 kbar. Geochimica et Cosmochimica Acta, 49, 865–870.

Holland, T.J.B. (1983) The experimental determination of activities in disordered and short-range ordered jadeitic pyroxenes. Contributions to Mineralogy and Petrology, 82, 214–220.

Inden, G. (1974) Ordering and segregation reactions in B.C.C. binary alloys. Acta Metallurgica, 22, 945–951.

Meiering, J.L. (1963) Miscibility gaps in ferromagnetic alloy systems. Philips Research Reports, 18, 318–330.

Phakey, P.P., and Ghose, S. (1973) Direct observation of anti-phase domain structure in omphacite. Contributions to Mineralogy and Petrology, 39, 239–245.

Wood, B.J., Holland, T.J.B., Newton, R.C., and Kleppa, O.J. (1980) Thermochemistry of jadeite-diopside pyroxenes. Geochimica et Cosmochimica Acta, 44, 1363–1371.

Manuscript received May 9, 1986
Manuscript accepted November 20, 1986